RSC Advances

ROYAL SOCIETY
OF CHEMISTRY

www.rsc.org/advances

RSC Advances
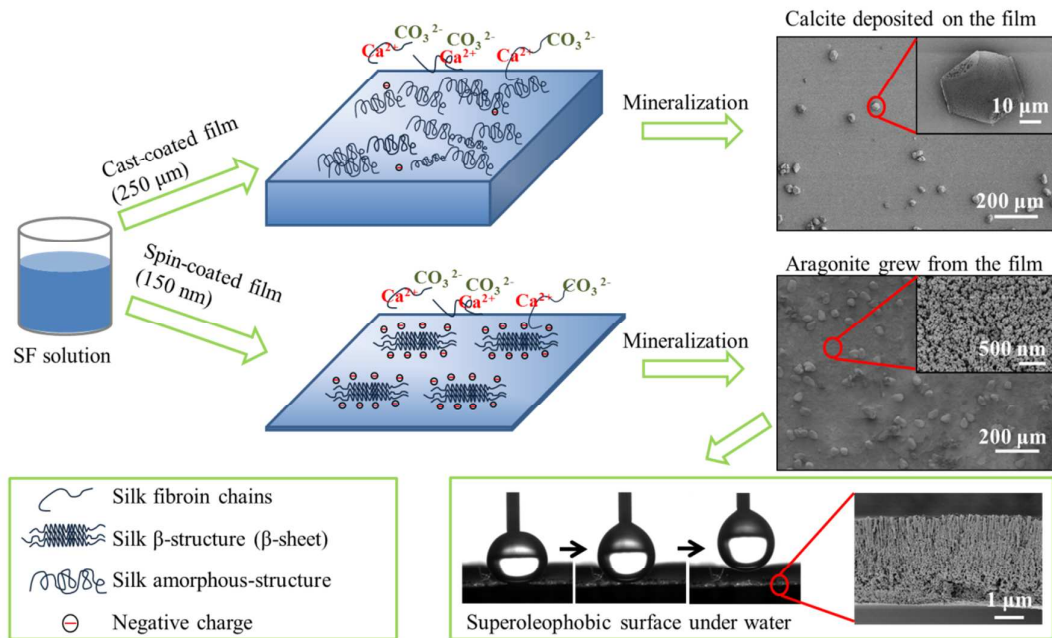
COMMUNICATION

Influences of Film Thickness and Fabrication Method on the Surface Structure and Mineralization-Templating of Silk Fibroin

Wei Hao,[a] David Porter[b] and Zhengzhong Shao[*a]

Abstract: The mineralization templating of *Bombyx mori* silkworm silk fibroin film on calcium carbonate is found to depend on the film thickness. Thin films promote oriented aragonite growth from the surface, which we show here to be due to β-sheet or β-strand morphology on the surface. Thick films with more random coil structure and hydrophobic groups give mainly the more thermodynamically stable calcite form. The surface structure and wettability of silk fibroin films are investigated in detail for the origin of such mediation effects.

Over the last few decades, the structure of biominerals and the properties of the organics involved in biomineralization processes have been extensively studied. For example, nacreous tablets have sophisticated hierarchical structures and remarkable properties, which are mediated by both the water-soluble fraction and the insoluble matrix of organic materials.[1] Previous work in the field tended to focus on the mineralization templating of water-soluble additives, while the influence of structure of a solid matrix still needs to be investigated in more detail. Insoluble templates in organisms can serves as a nucleation surface and guide inorganic crystals into remarkable forms.[1] As a result, although various inorganic minerals with multiscale topology can be prepared in an aqueous environment, the application of these insoluble templates to fabricate complex hybrid materials with specific surface functions was rarely reported.

Guided by previous research, *Bombyx mori* silk fibroin (SF) in an aqueous environment has proven extremely versatile in its control of the nucleation and growth of calcium carbonate ($CaCO_3$) aragonite phase, which we hypothesized to be due to the very good match between the β-strand structure of SF protein chains and the atomic spacing in the aragonite (010) plane, as outlined in Fig. S1.[2] In the presence of regenerated SF or other organic polymer solutions, degummed silk fibers[3] and chitosan films[4] were used as insoluble organic matrices to mediate $CaCO_3$ crystals deposited on the surfaces. However, the surface structures of these substrates were not studied, so we cannot identify which structure is best to mediate a specific inorganic mineral growing on a surface. Therefore, this study aimed to investigate the role of SF film surface structure in biomineralization, which might help our understanding of the function of insoluble organic matrices involved in biomineralization

processes in natural organisms. More specifically, we quantitatively test the previous hypothesis that β-strand structures can promote the crystallisation of aragonite over the more thermodynamically stable calcite form by using the chance observation that thinner films promote aragonite formation.

In this paper, we first investigate the influence of film thickness and fabrication methods on SF film surface mineralization. Then, we study the surface structures of different films using Fourier transform infrared attenuated total reflection (FTIR-ATR), specular refection infrared spectroscopy (FTIR-SR), measurement of surface energy components by contact angle, and X-ray photoelectron spectroscopy (XPS). Combining the surface structures with mineralization results on different SF films, we then investigate the mechanisms for oriented aragonite nucleation and growth on SF substrates. According to our best knowledge, there are few reports linking the characterization of the film surface structure and its mineralization properties. Moreover, based on this, we are try to control the structure and morphology of the inorganic layer to give the mineral surface some of the special characteristics of natural nacre, such as extreme wetting behavior and structural color.

SF films were prepared with a range of different thicknesses and production methods, as described in detail in Supporting Information. Crystallization of $CaCO_3$ on these different SF films has significantly different features, as shown in Fig. 1. Two main crystal forms observed on the film are calcite and aragonite, which were identified by Micro-Raman (Fig. S2). As general observations, the acicular aragonite seems to bond very closely with the SF film and appears to grow from the substrate (Fig. 1a~1c), whereas the irregular polyhedron calcite only has very limited connection with the substrate (Fig. 1d~1e). The calcite appears to adhere quite loosely to the surface where it is nucleated and then grow quite randomly.

Disc-like aragonite grew on spin-coated (SC) SF films with different thickness. The disc-like aragonite domains merged to form an aragonite layer on 150 nm spin-coated, SC, film (150 nm SC). The layer consisted of aragonite needles (Fig. 1a). When the film thickness was raised to 1 μm, the number of aragonite discs decreased (Fig. 1b). We observed that calcite only appeared on the 'optimum' 150 nm SC in the late stages of mineralization. This is consistent with our previous research,[2] where silk fibroin as an

additive in an aqueous environment can mediate the growth of aragonite, but when the SF in solution is depleted in the later stages, the thermodynamically more stable calcite is formed.

On cast-coated (CC) SF films, some aragonite grew on 1 µm CC (Fig. 1c), but rare aragonite on 10 µm CC (Fig. 1d). On increasing the thickness to 250 µm, we found only calcite deposited on the surface (Fig. 1e).

We placed a drop of water on the 150 nm SC film and looked at mineralization after the water had evaporated, and found an obvious difference in the $CaCO_3$ crystals deposited within and outside the water treated boundary (Fig. 1f~1h, Fig. S3). The area treated with water had much less aragonite grown on it (Fig. 1f) than the remaining area (Fig. 1g). 150 nm SC films treated with water were labelled here as 150 nm SCw.
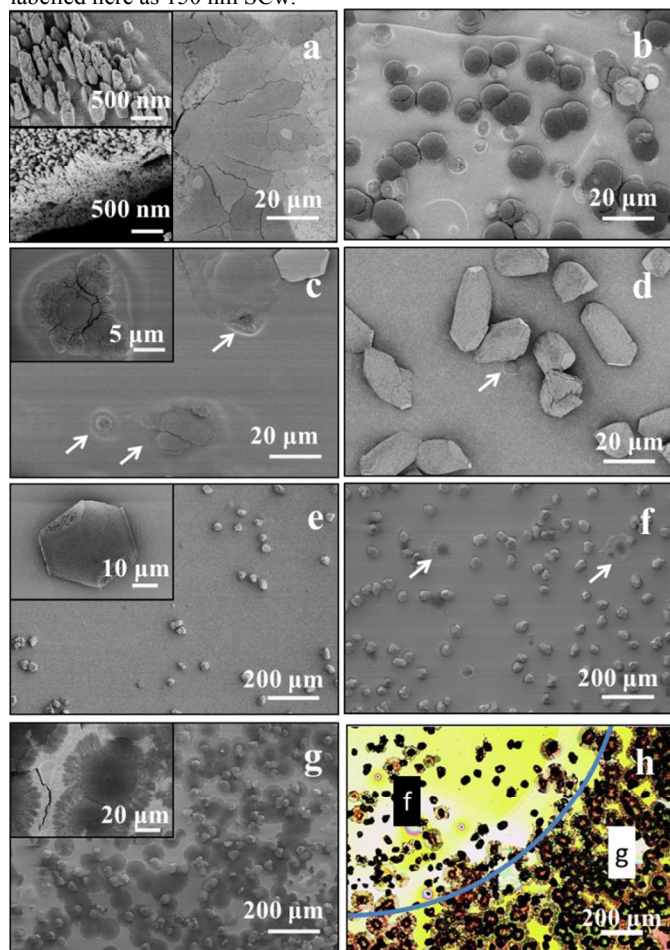
Fig. 1 FE-SEM images of aragonite and calcite grew on different SF films (a) 150 nm SC; (b) 1 µm SC; (c) 1 µm CC; (d) 10 µm CC; (e) 250 µm CC; and the area treated by a drop of water (f) or the remaining area (g) of 150 nm SC. (h) presents light microscope images of 150 nm SC locally treated by a drop of water; the arc represents the edge of the water treated area and the areas labelled "f" and "g" indicate SEM images from figures (f) and (g), respectively. White arrows in (c, d and f) indicated a small quantity of aragonite on the film.

To determine what caused the different mineralization results, we first investigated the conformational structure of the SF films by Fourier transform infrared (FTIR), which has been widely studied.[5] All of the films were characterized on the air-film surface. We focused on the amide I region between 1600 and 1700 cm^{-1}, which provides the most information on the structure of proteins. For our purposes, the amide I mode associated with random coil conformations give bands in the range of 1640-1650 cm^{-1}, and β-structures result in IR bands between 1620 and 1640 cm^{-1}.[6]

For 150 nm SC and 150 nm SCw, the films are too thin to be peeled off from silicon wafer, and silicon wafer has a strong infrared reflectance. So we can only choose specular refection (FTIR-SR) to characterize the films, as shown in Fig. 2 left. There was a slight distortion of the peak shape and a shift to lower frequency. It has been reported that the spectra of silkworm silk are different when using different FTIR spectroscopic techniques.[7] However, it allows us to compare the Amide I peak of different SC films.[8] To confirm the bands of random coil and β-sheet structure in FTIR-SR, we characterized SF films before and after methanol treatment. The 150 nm spin-coated film without methanol treatment could dissolve in water, and had a strong peak centered at 1631 cm^{-1} which was assigned to the amorphous structure. However, SR spectra of the methanol treated spin-coating films (150 nm SC and 150 nm SCw) showed a strong peak at 1617 cm^{-1}. This peak is characteristic of antiparallel β-structures. Therefore, we believe that β-structures were formed to a greater or lesser extent in the spin-coated films used in mineralization tests.

For 1 µm SC and all cast-coated SF films, the films are thick enough to peel from the substrates, and their surface structure can only be detected by attenuated total reflection (FTIR-ATR), as shown in Fig.2 (right). 1 µm spin-coated film showed an amide I band with a strong peak centered at 1620 cm^{-1} which reflected the β-structures. 1µm cast-coated film exhibited a new band at 1645 cm^{-1} that appeared in the spectra in addition to the peak at 1620 cm^{-1}. On increasing the thickness to 10 µm, and further to 250 µm, the 1645 cm^{-1} band increased significantly in intensity, which suggested that there was more disordered structure on the surface of thick films than the thin ones, and cast-coated over spin-coated.
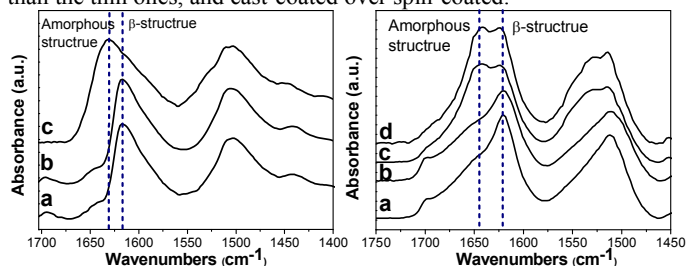
Fig. 2 SR spectra (left) of SF spin-coating film (a) 150 nm SC, (b) 150 nm SCw, (c) 150 nm SC before treatment with methanol. ATR spectra (right) of SF film (a) 1 µm SC, (b) 1 µm CC, (c) 10 µm CC. (d) 250 µm CC. Dashed lines show peak positions used to deduce structure in the text.

To quantify the charge characteristics of the surface energy of the films, we used contact angle measurements on specific films with standard liquids: water, methanamide and bromonaphthalene, of which two were polar and one was apolar. It could be seen that 150 nm SC had the lowest values for the more polar liquids (Table 1). Then, the surface energy was determined from the contact angle data using the Lifshitz-van der Waals/acid-base (LW/AB) approach,[6,9] as shown in Table 1. This method yields the total solid surface energy (γ_s^{TOT}) as the sum of the two components, γ_s^{LW} and γ_s^{AB} (i.e. $\gamma_s = \gamma_s^{LW} + \gamma_s^{AB}$), associated with electrodynamic Lifshitz-van der Waals (LW) interactions (apolar) and (Lewis) acid-base interactions (AB) (polar), respectively. γ_s^+ is the electron acceptor and γ_s^- is the electron-donor parameter of the polar component of the surface tension, $\gamma_s^{AB} = 2(\gamma_s^+ + \gamma_s^-)^{1/2}$.

The surface energy of SF is related to the periodic ordered structures on the SF films surface. It was found that Lewis acid–base components vary more than Lifshitz-van der Waals components

among the three films. Both γ_s^+ and γ_s^- decreased on increasing the film thickness. Increases in acid-base characteristics might reflect the greater availability of polar groups on the film surface.[10] The most significant result was that 150 nm SC had the highest basic parameter γ_s^- value. This implied that 150 nm SC had the highest surface basic polarity. These electron donating groups (perhaps the lone-paired oxygen atoms when considering the molecular structure) directed out of the film surface could attract Ca^{2+} ions to the surface to develop and grow. Moreover, increased γ_s^- implies decreased average size of the alkyl substituent R of poly (α-amino acids) and α-amino acid crystals.[11] Previous structural analyses of silk fibroin led to the proposal that the ordered regions (β-sheets or β-strands) are composed only of glycine, alanine and serine, while the amorphous regions contain the residues with large substituent R.[12] Therefore, it seemed reasonable to deduce that 150 nm SC had more β-structures and active sites on the surface than 150 nm SCw, while 250 μm CC had more amorphous structure on the surface.

Table 1 Contact angles of test liquids and surface free energy components and parameters on the air-film surface of different films

		150 nm SC	150 nm SCw	250 μm CC
Contact angles (°)	Water	59±1	66±1	77±2
	Methanamide	34±3	40±1	46±3
	Bromonaphthalene	19±4	21±3	21±2
Surface free energy components and parameters (in mJ/m^2)	γ_s^+	2.6±0.4	1.9±0.3	1.6±0.4
	γ_s^-	14.3±0.9	10.1±0.6	3.4±0.8
	γ_s^{AB}	12.1	8.7	4.7
	γ_s^{LW}	36.2±1.0	36.6±1.0	38.3±0.4
	γ_s^{TOT}	48.3	45.3	43.0

XPS is a surface-sensitive technique, allowing the outer surface of materials to be analyzed to a depth of several nanometers. The XPS spectrum of SF films presented the major photoelectron peaks located at binding energy values of 531 eV, 399 eV and 284.6 eV corresponding to the O(1s), N(1s), and C(1s) atomic orbitals, respectively. The chemical composition showed that there was a higher N/C ratio at the 150 nm SC surface (N/C=0.253) than 150 nm SCw (N/C=0.162) and 250 μm CC (N/C=0.013) (Table S1). Taking account of the oxygen content of the serine segments, the N/C and O/C ratios corresponded quite well with the -GAGAGS- motif of the ordered SF structures, and suggested that the ordered β-structures were preferred on the 150 nm SC surface, relative to the water treated one and CC films.

Fig. 3 shows the C1s high-resolution spectra of different film surfaces. The spectra were curve-fitted into five peaks at the binding energies of 284.6 eV (-C-C/H), 285.7 eV (-C-N), 286.4 eV (-C=O), 287.6 eV (O=C-N) and 288.6 eV (O=C-O-C/H).[13] O=C-N (287.6 eV) reflects the carbon on the peptide backbone, while -C-C/H (284.6) reflects the aliphatic C-C carbons of the amino acids pending groups. It could be seen that the peak associated with O=C-N backbone peptide groups (287.6 eV) of 150 nm SC is strongest among the three films, while 250 μm CC is the weakest. This indicated that more of these peptide backbone groups associated with β-structures are located at the surface than amorphous structures. This result suggested that 150 nm SC has the most β-sheets or β-strands, and the suppression of the peak at 287.6 eV was due to the dilution effect of disordered residues with large substituent R at the surface. This again suggested that the amorphous structure increases after 150 nm SC is treated with water, and 250 μm CC has the most amorphous structure among the three samples.
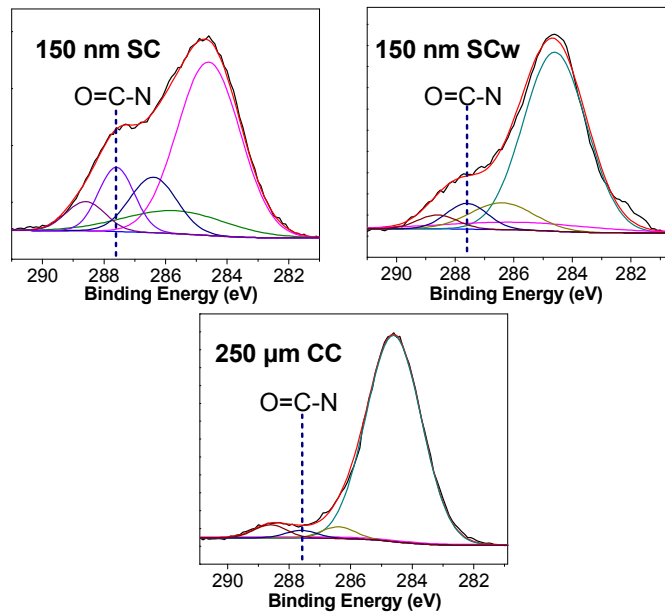
Fig. 3 Deconvolution of XPS C 1s core lever scan spectra of different SF film surfaces (original curves were marked with black lines). The 287.6 peak associated with the backbone O=C-N peptide group is marked by a line for reference.

Since our results implied that the β-sheet or β-strand structures on the surface of the SF film may have a templating effect on the growth of aragonite, a short series of comparative experiments were conducted to enhance or deplete the fraction of β-structures at the surface. First, we used 5 M lithium bromide as a chaotropic agent (which can change the highly ordered silk II structure to silk I[14]) to treat the 250 μm CC for 10 min, and then the mineralization was carried out by using the same procedure. Fig. 4a and Fig. S4 showed that only the calcite was deposited on the film and no aragonite grew on the surface.

Conversely, we used chymotrypsin to treat the 250 μm CC to expose more β-sheet structures on the surface.[15] Chymotrypsin has been widely used to biodegrade the noncrystalline regions of fibroin fibers to obtain highly crystalline fibroin protein structure.[16] The sample was examined by FTIR, and a sharp β-sheet peak was observed at 1619 cm^{-1} of the Amide I region (Fig. S5). Compared with 250 μm CC, the chymotrypsin treated sample lost much of its disordered components. After mineralization under the same procedure, two kinds of disk with diameters around 25 μm and 60 μm appeared on the film (Respectively shown in the up and down inset of Fig. 4b). Results from Raman spectra showed that the polymorphs of the small and large disks of $CaCO_3$ were aragonite and vaterite, respectively (Fig. S8).
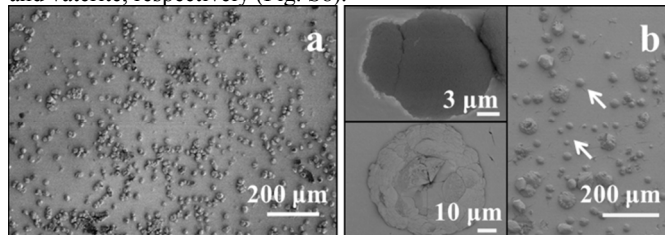
Fig. 4 FE-SEM images of (a) calcite deposited on 250 μm CC treated by 5M LiBr for 10min; (b) aragonite and vaterite deposited on 250 μm CC treated by treated by 10 U/ mL chymotrypsin for 12 h. White arrows in (b) indicated aragonite on the film.

COMMUNICATION

Taken together, these observations provided evidence that the preferential aggregation of CaCO$_3$ was controlled by the oriented aligned β-sheet structures on the SF film. This supported the hypothesis in our previous study, namely that the β-structures (-sheet or -strand) of silk fibroin possess an intrinsic preferential ability to induce the crystallization of the aragonite phase.[2, 3] Moreover, in the present system, both the insoluble matrix template (SF film) and the soluble functional molecule (aqueous SF) are required to regulate the crystallization of CaCO$_3$, which was demonstrated in control experiments: significant amounts of conventional calcite and very little aragonite was deposited on the SF film in the absence of silk fibroin chains in the solution, and both the calcite and aragonite had very limited connection with the substrate (Fig. S7a). On the other side, conventional calcite with decorated angles was produced on the bare silicon wafer in silk fibroin solution (Fig. S7b), demonstrating the need for the SF film template.

Film thickness is not the only factor that controls crystal growth, and we need to consider briefly the role of molecular orientation due to film production methods. We noticed that spin-coating is not the only film production route for growing aragonite on the surface. Aragonite can be produced on an SF film cast-coated on silicon with about 200 nm thickness (Fig. S8), but the growth direction is more irregular. Centrifugal force can make the SF chains more radially oriented on the surface. Moreover, if we coated a film (80 nm thickness) with a blade on the silicon placed on an electric heating plate, we found that aragonite discs were oriented in the direction of the blade movement after mineralization (Fig. S9), due to the SF macromolecules being oriented by the shear forces induced in the film by the blade. This is similar to previous research, where aragonite could grow on the surface of silk fiber with strong orientation along the longitudinal axis.[3] The results suggested that ordered surface structure on the film surface could mediate oriented deposition of the mineral.

Our observations suggest that thin spin-coated films, especially for 150 nm SC, have the correct charge and β-morphology (-sheet or -strand) on the surface to template aragonite, while thicker cast-coated films have more random coil on the surface. The reasons for these differences are due mainly to two factors: film thickness and fabrication method. For different film thickness, it has been reported that random coils are more favored than β-sheet structures at the interface because they effectively minimize the interfacial free energy by rendering the polymer surface hydrophobic.[6] Longer drying times of thicker films allow hydrophilic polar groups to be pulled inside the film surface by the strong water affinity to leave a hydrophobic surface. One possibility is that the structure on a thick film surface is similar to the three-fold helical conformation discovered at the air-water interface by Gido et al,[17] which cannot nucleate the crystal growth.

In comparison, drying rate for thinner films is too fast to let the SF macromolecules rearrange, which can leave more β-sheet structures and hydrophilic groups exposed on the film surface. Moreover, the thicknesses of 150 nm SC is comparable to the extended length of the domains and can impose severe limitations on the unfolding behavior.[18] However, when a thin film surface is exposed to water, the oriented chains on the film surface can relax into an equilibrium disordered random coil state with longer drying time and more swelling room, which again cannot template the crystals due to the incorrect intermolecular distances.

For different fabrication methods, spin-coated films can be dried in a very short time. Moreover, the centrifugal force of spin coating can stretch the silk backbone chains and expose more hydrophilic groups on the surface. Since, 150 nm SC cannot be peeled off from silicon wafer, the bonding force might also prevent the rearrangement of SF macromolecules.

During our investigations, we have found that hybrid layers can give the mineralised film a number of special properties. Surfaces with an oriented aragonite layer are superoleophobic under water without any other treatment, just like a clam's shell and fish skin (Fig. S10). Compared with micro/nano-hierarchical perfluorinated structures, these superoleophobic surfaces are more stable underwater, may giving the surface an underwater self-cleaning property. This potentially provides a solution to the problem of oil contamination on metal ships and other aquatic equipment.[19] Moreover, the oriented aragonite needles are several hundred nanometer in length, having the same order of size as the light wavelength. This can give the surface structural color (Fig. S11), similar to photonic-crystal structure coloration.[20]

In summary, the combination of observations presented here validate the hypothesis that β-structure (-sheet or -strand) is the key factor for mediating aragonite growth on an SF film surface. Thick SF films do not have this templating capability because of more disordered random coil conformers and hydrophobic groups on the surface, even after treatment with methanol. Thin SF spin-coated films having oriented β-morphology (-sheet or -strand) on the surface that can be optimized in their dying rate and centrifugal force through the film thickness to afford nucleation sites and a molecular growth template for aragonite. This is an excellent example of optimizing the fabrication conditions to produce an organic/inorganic composite material. The aragonite nano-needles depositing on the solid template can enhance the surface roughness and endow special superoleophobic and optical properties.

Notes and references

[a] State Key Laboratory of Molecular Engineering of Polymers, Advanced Materials Laboratory, Department of Macromolecular Science, Fudan University, Shanghai, 200433, People's Republic of China. E-mail: zzshao@fudan.edu.cn

[b] Department of Zoology, University of Oxford, South Parks Road, Oxford OX1 3PS, UK.

† Electronic Supplementary Information (ESI) available: [Experimental section, and the detailed characterization data of the prepared materials including Raman, FTIR, water contact angle, SEM, Light Microscope images are included]. See DOI: 10.1039/c000000x/

1. L. Addadi, D. Joester, F. Nudelman and S. Weiner, *Chemistry-A European Journal*, 2006, **12**, 980-987; Y. Levi-Kalisman, G. Falini, L. Addadi and S. Weiner, *J. Struct. Biol.*, 2001, **135**, 8-17.
2. T. Wang, D. Porter and Z. Z. Shao, *Adv. Funct. Mater.*, 2012, **22**, 435-441.
3. C. Cheng, Y. Yang, X. Chen and Z. Shao, *Chem. Commun.*, 2008, 5511-5513.
4. Y. Wu, C. Cheng, J. Yao, X. Chen and Z. Shao, *Langmuir*, 2011, **27**, 2804-2810; A. Sugawara and T. Kato, *Chem. Commun.*, 2000, 487-488.
5. S. Ling, Z. Qi, D. P. Knight, Z. Shao and X. Chen, *Polymer Chemistry*, 2013, **4**, 5401-5406; H. Wang and Y. Zhang, *Soft Matter*, 2013, **9**, 138-145.
6. O. N. Tretinnikov and Y. Tamada, *Langmuir*, 2001, **17**, 7406-7413.
7. E. Van Nimmen, K. De Clerck, J. Verschuren, K. Gellynck, T. Gheysens, J. Mertens and L. Van Langenhove, *Vibrational Spectroscopy*, 2008, **46**, 63-68.
8. X. Ma and X. Ni, *Langmuir*, 2014, **30**, 2241-2248.

9. C. J. van Oss and R. J. Good, *Journal of Macromolecular Science—Chemistry*, 1989, **26**, 1183-1203.

10. M. Kim, J. C. Kim, Y. Rho, J. Jung, W. Kwon, H. Kim and M. Ree, *J. Mater. Chem.*, 2012, **22**, 19418-19428.

11. S. Spange, C. Schmidt and H. R. Kricheldorf, *Langmuir*, 2001, **17**, 856-865.

12. C. Fu, Z. Shao and V. Fritz, *Chemical Communications*, 2009, 6515-6529.

13. L. Zhou, X. Chen, W. Dai and Z. Shao, *Biopolymers*, 2006, **82**, 144-151; H. J. Jin, J. Park, R. Valluzzi, P. Cebe and D. L. Kaplan, *Biomacromolecules*, 2004, **5**, 711-717; M. Liang, J. Yao, X. Chen, L. Huang and Z. Shao, *Materials Science & Engineering C-Materials for Biological Applications*, 2013, **33**, 1409-1416.

14. Y. Shen, M. A. Johnson and D. C. Martin, *Macromolecules*, 1998, **31**, 8857-8864.

15. X. Hu, Q. Lu, D. L. Kaplan and P. Cebe, *Macromolecules*, 2009, **42**, 2079-2087.

16. M. Li, M. Ogiso and N. Minoura, *Biomaterials*, 2003, **24**, 357-365.

17. R. Valluzzi, S. P. Gido, W. P. Zhang, W. S. Muller and D. L. Kaplan, *Macromolecules*, 1996, **29**, 8606-8614; R. Valluzzi, S. P. Gido, W. Muller and D. L. Kaplan, *International Journal of Biological Macromolecules*, 1999, **24**, 237-242.

18. H. J. Jin and D. L. Kaplan, *Nature*, 2003, **424**, 1057-1061.

19. X. L. Liu, J. Zhou, Z. X. Xue, J. Gao, J. X. Meng, S. T. Wang and L. Jiang, *Adv. Mater.*, 2012, **24**, 3401-3405.

20. J. Zi, X. D. Yu, Y. Z. Li, X. H. Hu, C. Xu, X. J. Wang, X. H. Liu and R. T. Fu, *Proc. Natl. Acad. Sci. U. S. A.*, 2003, **100**, 12576-12578.